Lo nog in review

IET Renewable Power Generation

Power absorption by closely spaced point absorbers in constrained conditions

Journal:	*IET Renewable Power Generation*
Manuscript ID:	Draft
Manuscript Type:	Research Paper
Date Submitted by the Author:	
Complete List of Authors:	De Backer, Griet; Ghent University, Department of Civil Engineering Vantorre, Marc Beels, Charlotte De Rouck, Julien Frigaard, Peter
Keyword:	array, multiple bodies, point absorber, wave energy

Power absorption by closely spaced point absorbers in constrained conditions

G. De Backer[1a], M. Vantorre[1b], C. Beels[1a],
J. De Rouck[1a], P. Frigaard[2]

November 27, 2009

[1a] Coastal Engineering Division - [1b] Maritime Technology Division
Department of Civil Engineering, Ghent University
Technologiepark Zwijnaarde 904, 9052 Zwijnaarde, Belgium
[2] Department of Civil Engineering, Aalborg University
Sohngaardsholmsvej 57, 9000 Aalborg, Denmark

Corresponding author: Marc Vantorre
E-mail: marc.vantorre@ugent.be

Abstract

The performance of an array of closely spaced point absorbers is numerically assessed in a frequency domain model. Each point absorber is restricted to the heave mode and is assumed to have its own linear power take-off system. Unidirectional irregular incident waves are considered, representing the wave climate at Westhinder on the Belgian Continental Shelf. The impact of slamming, stroke and force restrictions on the power absorption is evaluated and optimal power take-off parameters are determined. For multiple bodies optimal control parameters are not only dependent on the incoming waves, but also on the position and behaviour of the other buoys. Applying the optimal control values for a single buoy to multiple closely spaced buoys results in a suboptimal solution for the array. Other ways to determine the power take-off parameters are diagonal optimization and individual optimization. These methods are applied to two array layouts consisting of twelve buoys in a staggered grid and 21 buoys in an aligned grid. Compared to diagonal optimization, it was found that individually optimizing the control parameters increased the energy absorption at Westhinder with about 16 % to 18 % for the two layouts, respectively.

Keywords: array, multiple bodies, point absorber, wave energy

Nomenclature

b_{ext} = external damping coefficient [kg/s]

B_{ext} = external damping matrix (NxN) [kg/s]

B_{hyd} = hydrodynamic damping matrix (NxN) [kg/s]

d = buoy draft [m]

D = buoy waterline diameter [m]

f = wave frequency [Hz]

F = force [N]

I = identity matrix (NxN) [-]

K = stiffness matrix (NxN) [kg/s^2]

H = wave height [m]

m = buoy mass [kg]

m_{sup} = supplementary mass [kg]

M = buoy mass matrix (NxN) [kg]

M_a = added mass matrix (NxN) [kg]

M_{sup} = supplementary mass matrix (NxN) [kg]

N = number of buoys [-]

n_f = number of frequencies [-]

q = ratio of maximum power absorption by N interacting bodies to N isolated bodies [-]

$\tilde{q}$ = power absorption ratio of N interacting bodies and N isolated bodies in suboptimal conditions [-]

S = frequency spectrum [m^{2}s]

t = time [s]

T = wave period [s]

z = buoy position [m]

Z = buoy position vector (Nx1)[m]

γ = peak enhancement factor [-]

ζ = wave elevation [m]

σ = spectral width parameter [-]

ω = angular frequency [rad^{-1}]

Subscripts

A = amplitude

abs = absorbed

ex = exciting

f = frequency

max = maximum value

s, $sign$= significant

1 Introduction

Point absorbers are oscillating wave energy converters with dimensions that are small compared to the incident wave lengths. In order to absorb a considerable amount of power, several point absorbers are grouped in one or more arrays. Some point absorber devices under development are composed of a large structure containing multiple, closely spaced oscillating bodies. Examples are Wave Star [1], Manchester Bobber [2] and FO^3 [3].

Several theoretical models dealing with interacting bodies have been developed. Budal [4], Evans [5] and Falnes [6] adopted the 'point absorber approximation' to derive expressions for the maximum power an array can absorb. The approximation relies on the assumption that the bodies are small compared to the incident wave lengths, so the wave scattering within the array can be neglected while calculating the interactions. This means that the exciting forces on the fixed devices are equal to those of isolated bodies. The scattering of the radiated waves within the array is also neglected. The point absorber theory gives good results for $k_w R << 1$, with k_w the wavenumber (= $2\pi/L$) and R the floater radius [7]. A theory accounting more accurately for the body interactions is the 'plane-wave approximation' [8–10], which is based on the assumption that the bodies are widely spaced relative to the incident wavelengths, so the radiated and circular scattered waves can be locally approximated by plane waves. For closely spaced bodies, which is the focus of this paper, this theory is not suitable as the wide spacing requirement is not fulfilled, except for very short wave lengths. Satisfying computation results are obtained with this method for values of $k_w d_{cc}$ larger than unity [9, 11], where d_{cc} denotes the centre-to-centre spacing between two neighbouring bodies. In the majority of studies, both theories have been applied to arrays for unconstrained conditions. Contrary to the point absorber approximation, the plane wave approximation is also suitable to study the power absorption of an array in suboptimal conditions, as scattering might be relatively important in that case [8,12]. Heaving point absorbers with constrained displacements have been studied by McIver [12, 13] by means of the plane wave approximation and by Thomas and Evans [14] with the point absorber approximation, although less suitable. Motion restrictions appeared to significantly reduce the power absorption capability of the array for longer wave lengths [12]. Apart from regular waves, McIver et

al. [13] also studied array interactions in irregular unidirectional and directionally spread seas for a varying number of oscillators between 5 and 20, arranged in one or two lines. In unidirectional irregular normal waves, the power absorption in unconstrained motions outperforms the power extraction in constrained motions. In multidirectional seas, this effect seemed to be clearly less pronounced.

More exact results on array hydrodynamics can be obtained by the 'multiple scattering' theory of Mavrakos [15]. This theory has been extensively compared with the above mentioned approximate theories (the point absorber approximation and plane wave approximation) [7, 16].

With current computer capacity, Boundary Element Methods (BEM) are becoming more and more important to investigate interacting point absorbers. Ricci et al. [17] compared results obtained with a BEM code to the point absorber approximation and optimized the point absorber geometry and interbody distance of two array configurations, each consisting of 5 floaters in irregular waves with and without directional spreading. Taghipour et al. [3] investigated the interaction of 21 heaving point absorbers in a floating platform, known as the FO^3 device, in unconstrained conditions. By means of a mode expansion method, he was able to reduce the computation time to calculate the body responses by a factor of 10 to 15. Thomas et al. [14] validated numerical simulations, predicting the response amplitude of the floater motions of interacting hemispherical floaters using the BEM package WAMIT [18], with experimental tests based on line array configurations. Recently, Cruz et al. [19] numerically investigated the performance of an array layout composed of four heaving cylinders subject to passive control. Babarit et al. [20] assessed the interaction between two heaving cylinders with hydraulic power take-off systems in a time domain model.

The impact of constraints on a single point absorber has been studied by De Backer et al. [21], showing that stroke and force restrictions might have a significant impact on the power absorption. In [22] the influence of slamming and stroke restrictions as well as limitations to the control forces are investigated for an array in a frequency domain model with input from WAMIT on the hydrodynamics. The control parameters are optimized with different strategies. In this paper, the results are further extended. The optimization strategies are evaluated for two different array layouts and their energy absorption is assessed at Westhinder on the Belgian Continental Shelf.

2 Methodology

2.1 Equation of motion

The equation of motion of a point absorber, oscillating in heave mode, is expressed by Newton's second law:

$$m\ddot{z} = F_{ex} + F_{rad} + F_{res} + F_{damp} + F_{tun} \tag{1}$$

where m is the mass of the buoy and $\ddot{z}$ its acceleration. F_{ex} is the exciting force, F_{rad} the radiation force, F_{res} the hydrostatic restoring force, F_{damp} the external damping force to extract power and F_{tun} the tuning force for phase-controlling the buoy. The damping force is delivered by the power take-off (PTO) system, whereas the tuning force can be exerted by the PTO or another control mechanism. For simplicity, the PTO is assumed linear.

The equation of motion of N multiple bodies, oscillating in heave in a regular wave with angular frequency ω, can be expressed as follows with linear theory in the frequency domain:

$$-\omega^2(\mathbf{M}+\mathbf{M_a}(\omega)+\mathbf{M_{sup}})\,\hat{\mathbf{Z}}+j\omega(\mathbf{B_{ext}}+\mathbf{B_{hyd}}(\omega))\,\hat{\mathbf{Z}}+\mathbf{K}\hat{\mathbf{Z}}=\hat{\mathbf{F}}_{\mathbf{ex}}(\omega) \tag{2}$$

where $\hat{\mathbf{Z}}$ is the complex amplitude of the buoy positions, $\mathbf{M}$ the mass matrix of the buoys, and $\mathbf{K}$ the matrix with hydrostatic restoring coefficients or stiffness matrix. The added mass matrix and hydrodynamic damping matrix are denoted by $\mathbf{M_a}$ and $\mathbf{B_{hyd}}$, respectively. They are both symmetric N x N matrices with the hydrodynamic interaction coefficients on the non-diagonal positions. The vector $\hat{\mathbf{F}}_{\mathbf{ex}}$ contains the complex amplitudes of the heave exciting forces. The hydrodynamic parameters $\mathbf{M_a}$, $\mathbf{B_{hyd}}$ and $\hat{\mathbf{F}}_{\mathbf{ex}}$ are obtained from the BEM software WAMIT [18]. Since the natural frequency of the buoys is generally smaller than the incident wave frequencies, the buoys are often tuned towards the characteristics of the incident waves to augment power absorption. This can be effectuated by latching techniques [23], by introducing a supplementary spring term [17] or a supplementary mass term [24]. In this paper, a tuning force proportional to the acceleration has been implemented by means of a supplementary mass matrix, $\mathbf{M_{sup}}$. $\mathbf{M_{sup}}$ is a diagonal matrix, containing the supplementary mass coefficients of each buoy on the diagonal: $\mathbf{M_{sup_{jk}}} = m_{sup}^{(j)}\,\mathbf{I_{jk}}$, with $m_{sup}^{(j)}$ the supplementary mass for buoy j, $\mathbf{I}$ the NxN identity matrix and $j,k \in [1,N]$. A linear external damping matrix, $\mathbf{B_{ext}}$, has been applied, enabling power extraction. The external damping matrix -also a diagonal matrix- is defined as: $\mathbf{B_{ext_{jk}}} = b_{ext}^{(j)}\,\mathbf{I_{jk}}$.

The superposition principle is used to obtain the time-averaged power absorption in irregular waves:

$$\mathbf{P_{abs}} = \sum_{i=1}^{n_f} \frac{1}{2}\omega_i^2 \mathbf{Z_i^*} \mathbf{B_{ext}} \mathbf{Z_i} \tag{3}$$

where n_f is the number of frequencies and $\mathbf{Z_i^*}$ the complex conjugate transpose of $\mathbf{Z_i}$. The calculations are performed for 40 frequencies, ranging between 0.035 and 0.300 Hz. All buoys are assumed to be equipped with their own power take-off system.

2.2 Constraints

Slamming constraint

Slamming is a phenomenon that occurs when the buoy re-enters the water, after having lost contact with the water surface. The buoy experiences a slam, which may result in high hydrodynamic pressures and loads. These impacts have a very short duration, with a typical order of magnitude of milliseconds. However, they may cause local plastic deformation of the material [25]. Fatigue by repetitive slamming pressures can be responsible for structural damage of the material. For this reason, a restriction has been implemented, requiring that the significant amplitude of each buoy position relative to the free water surface elevation should be smaller than a fraction α of the draft d of the buoy:

$$(z^{(j)} - \zeta^{(j)})_{A,sign} \leq \alpha \cdot d \tag{4}$$

where $z^{(j)}$ is the position of buoy j, $\zeta^{(j)}$ the water elevation at the center of buoy j and α a parameter that is arbitrarily chosen equal to one. The water elevation has been determined with the incident wave only, thereby neglecting the radiated and diffracted waves from buoy j as well as from the other buoys.

This slamming restriction might require a decrease of the tuning parameter m_{sup} and/or an increase of the external damping coefficient b_{ext}. Not only the occurrence probability of slamming will be reduced by this measure, but also the magnitude of the associated impact pressures and loads will drop, since they are dependent on the impact velocity of the body relative to the water particle velocity and this impact velocity will decrease when the control parameters of the buoy are adapted according to the restriction imposed.

Stroke constraint

In practice, many point absorber devices are very likely to have restrictions on the buoy motion, e.g. imposed by the limited height of the rams in case of a hydraulic conversion system or by the limited height of a platform structure enclosing the oscillating point absorbers. Therefore a stroke constraint is implemented, imposing a maximum value on the significant amplitude of the body motion:

$$z^{(j)}_{A,sign} \leq z^{(j)}_{A,sign,max} \tag{5}$$

With the position spectrum defined as: $S^{(j)}_{z_i} = z^{(j)2}_{A,i}/2\Delta f$, the significant amplitude of the buoy motion can be obtained from $z_{A,sign} = 2\sqrt{\int_{i=1}^{n_f} S^{(j)}_{z,i} \cdot \mathrm{d}f}$. Hence, the constraint on the significant amplitude of the buoy motion is not an absolute constraint, but a restriction associated with a statistical exceedance probability. In the examples that will be presented in this paper, a maximum value of the significant amplitude of 2.00 m is chosen. Assuming Rayleigh distribution of the buoy motions, this restriction means that a stroke of 4.90 m is exceeded for 5.0 % of the waves. The implementation of constraints on the

body motion increases the reliability of the linear model, which is based on the assumption of small body motions.

Force constraint

In some cases, the optimal control parameters for maximum power absorption, result in very large control forces. The tuning force, in particular, might become very large and can even be a multiple of the damping force. If this tuning force is to be delivered by the PTO, it might result in a very uneconomic design of the PTO system. For this reason it is interesting to study the response of the floaters in case the total control force is restricted. If the force spectrum is expressed as: $S_{F,i}^{(j)} = F_{A,i}^{(j)2}/2\Delta f$ and the significant amplitude of the force is defined as $F_{A,sign}^{(j)} = 2\sqrt{\int_{i=1}^{n_f} S_{F,i}^{(j)} \cdot \mathrm{d}f}$, then the significant amplitude of the damping and tuning force, respectively, for buoy j are given by:

$$F_{bext,A,sign}^{(j)} = 2\sqrt{\int_0^\infty S_{F_{bext,A}}^{(j)}(f)\mathrm{d}f} \tag{6}$$

$$F_{msup,A,sign}^{(j)} = 2\sqrt{\int_0^\infty S_{F_{msup,A}}^{(j)}(f)\mathrm{d}f} \tag{7}$$

The significant amplitude of the total force, expressed in Eq. (8) will be limited to 200 kN.

$$F_{tot,A,sign}^{(j)} = 2\sqrt{\int_0^\infty \left(S_{F_{bext,A}}^{(j)}(f) + S_{F_{msup,A}}^{(j)}(f)\right)\mathrm{d}f} \tag{8}$$

2.3 Optimization strategies

The relative performance of an array is often expressed by means of the 'q-factor', defined as the maximum time-averaged total power absorbed by the N bodies in the array divided by N times the maximum time-averaged power absorption by a single point absorber:

$$q = \frac{P_{\text{abs, max by array of } N \text{ floaters}}}{N \cdot P_{\text{abs, max by an isolated floater}}} \tag{9}$$

The q-factor expresses the performance of the array compared to isolated buoys in ideal circumstances, i.e. when optimal tuning is assumed. Since the control parameters are optimized for a certain sea state, rather than for a particular frequency, the power absorption will be suboptimal, even in unconstrained conditions. Hence, for the current purpose, a measure is needed to express and compare the efficiency of different optimization strategies applied to a given array in suboptimal conditions. Therefore a gain factor $\tilde{q}$ is defined as the ratio of the total power absorbed by the array to the power absorbed by the point absorbers in isolation, subjected to the same constraints.

Three strategies to determine the control parameters for multiple bodies will be compared: optimal control parameters from a single body, diagonal optimization and individual optimization.

2.3.1 Optimal control parameters from a single body

In the first strategy, the optimal control parameters from a single body (OPSB) are applied to all the bodies in the array. It should be kept in mind that 'optimal parameters' in this case means that these parameters lead to the maximum possible power absorption within the imposed constraints and with the described control and hence they do not necessarily give the absolute maximum power absorption capability of the body. With this method all bodies have the same control coefficients. However, the control forces, $\mathbf{M_{sup}}\ddot{\mathbf{Z}}$ and $\mathbf{B_{ext}}\dot{\mathbf{Z}}$, are not similar for the different buoys, since the buoy velocities and accelerations differ in amplitude and phase. If $m_{sup,SB}$ and $b_{ext,SB}$ are the single body optimal parameters for a specific sea state and a certain combination of restrictions, then the absorbed power for the array is obtained with the following control matrices:

$$\mathbf{M_{sup}} = m_{sup,SB}\,\mathbf{I} \text{ and } \mathbf{B_{ext}} = b_{ext,SB}\,\mathbf{I} \tag{10}$$

2.3.2 Diagonal optimization

With the second technique, all the buoys still get the same parameters, but they are optimized with a simplex search (SS) method for unconstrained conditions and a sequential quadratic programming (SQP) method for constrained conditions. The methods are validated with an exhaustive searching (ES) method. The latter method gives the same results as SS and SQP, however, SS and SQP are much faster, which is important if very accurate results need to be obtained. The supplementary mass matrix and external damping matrix are similar to those in Eq. (10), but $m_{sup,DO}$ and $b_{ext,DO}$ are determined so that the total absorbed power is maximal for the specific array (within the constraints). This technique is called diagonal optimization (DO). It is also referred to as scalar optimization [17].

$$\mathbf{M_{sup}} = m_{sup,DO}\,\mathbf{I} \text{ and } \mathbf{B_{ext}} = b_{ext,DO}\,\mathbf{I} \tag{11}$$

2.3.3 Individual optimization

With the last technique the floaters are individually optimized (IO), i.e. for every floater separate values of $m_{sup}^{(j)}$ and $b_{ext}^{(j)}$ are determined. Note that the control matrices are still diagonal matrices, however with non-identical elements on the diagonal:

$$\mathbf{M_{sup}} = \begin{bmatrix} m_{sup}^{(1)} & & & \\ & m_{sup}^{(2)} & & \\ & & \ddots & \\ & & & m_{sup}^{(N)} \end{bmatrix}, \ \mathbf{B_{ext}} = \begin{bmatrix} b_{ext}^{(1)} & & & \\ & b_{ext}^{(2)} & & \\ & & \ddots & \\ & & & b_{ext}^{(N)} \end{bmatrix} \tag{12}$$

IO has only been successfully applied in constrained conditions. The optimization is carried out with a SQP method only, since a simple exhaustive searching method would require too much CPU-time. If $n_{m_{sup}}$ and $n_{b_{ext}}$ values of $m_{sup}^{(j)}$ and $b_{ext}^{(j)}$, respectively, are to be evaluated, the calculation of the total power absorption needs to be performed $(n_{m_{sup}} \cdot n_{b_{ext}})^N$ times. If e.g. 40 values for each control parameter are to be assessed for a configuration of e.g. 12 floaters, the required number of power absorption calculations would be $2.8 \cdot 10^{38}$, which is not feasible. A drawback of the SQP algorithm for individual tuning is that it might converge to a local maximum, depending on the initial conditions. Hence, the choice of the initial conditions is very important. The control parameters from diagonal optimization have been used as initial values from which individual tuning parameters are obtained. It is advised to check the output with simulations based on different starting values. For instance, the control parameters obtained with individual optimization in a slightly less or more energetic sea state can also be used as begin values. If the number of buoys were small (preferably smaller than 6), the SQP algorithm could be executed with a set of initial conditions for $m_{sup}^{(j)}$ and $b_{ext}^{(j)}$ (multistart algorithm) to increase the chance of reaching the absolute maximum value. Unfortunately, a multistart application is much too time-consuming for the configurations that will be investigated in this paper, even if only two initial values per parameter are selected.

3 Case study specifications

3.1 Configuration

Two multiple body layouts are considered, an aligned grid configuration with 21 buoys, as presented by Fred Olsen and applied to the FO^3 device [3], and a staggered grid configuration with 12 buoys. The layouts are shown in Figures 1(a) and 1(b), respectively. The buoys are placed in a square, fixed structure with four supporting columns at the edges. However, the effects of diffraction and reflection of waves on the columns will be further neglected in this study. The interdistance between two successive rows is 8.0 m and 6.5 m, respectively. The incoming waves propagate in the direction of the x-axis, as indicated on the Figures. The buoys are assumed to oscillate in heave mode only. In Figures 2(a) and 2(b) the buoy geometry is presented. A buoy consists of a cone shape with apex angle 90° and a cylindrical upper part with a diameter of 4 m for the configuration with 21 buoys and a diameter of 5 m for the array with 12 buoys. The equilibrium draft of the buoys is 2.5 and 3.0 m, respectively. The total submerged volume, which can be a measured for

the material cost, is approximately the same for both configurations. However, it is expected that the total component cost of the array with 12 floaters will be less than for the grid with 21 buoys, since less power take-off units are required. Most results are presented for the configuration with 12 buoys.

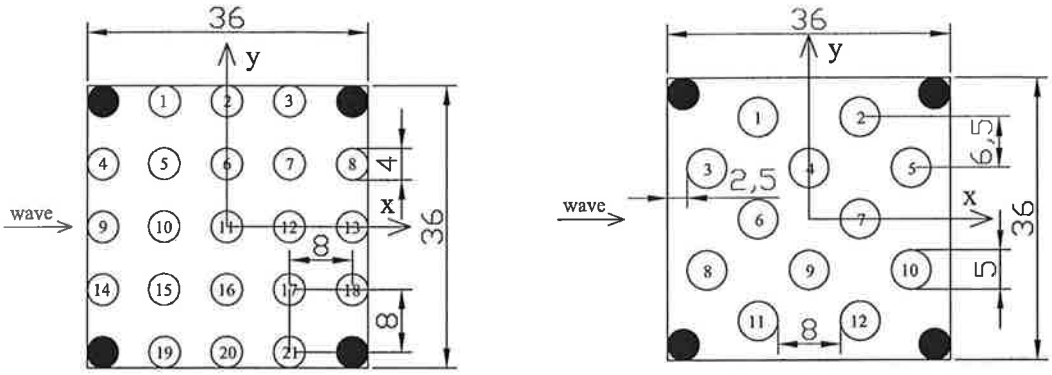

(a) Configuration with 21 buoys in an aligned grid.

(b) Configuration with 12 buoys in a staggered grid.

Figure 1: Array layout, dimensions in m.

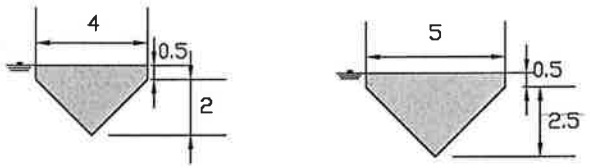

(a) Buoy geometry for the configuration with 21 buoys.

(b) Buoy geometry for the configuration with 12 buoys.

Figure 2: Point absorber geometry, dimensions in m.

3.2 Wave climate

Eight sea states are defined based on scatter diagrams from buoy measurements at Westhinder, on the Belgian Continental Shelf. The sea states with their corresponding occurrence probabilities (OP) are displayed in Table 1. The mean water depth at the Westhinder buoy is 28.8 m. The majority of calculations will be carried out for the fifth sea state, characterized by a significant wave height, H_s = 2.25 m and peak period, T_p = 7.22 s. The generated spectrum is based on a parameterized JONSWAP spectrum [26].

Table 1: Sea states and occurrence probabilities at Westhinder based on measurements from 1-7-1990 until 30-6-2004 (Source of original scatter diagram: Flemish Ministry of Transport and Public Works (Agency for Maritime and Coastal Services, Coastal Division)).

Sea state	H_s [m]	T_p [s]	OP [%]
1	0.25	5.24	21.58
2	0.75	5.45	37.25
3	1.25	5.98	22.02
4	1.75	6.59	10.65
5	**2.25**	**7.22**	**5.14**
6	2.75	7.78	2.27
7	3.25	8.29	0.79
8	3.75	8.85	0.21

4 Results

4.1 Unconstrained

In this Section, simulations are presented for unconstrained point absorber motions and control forces on the configuration with 12 buoys. Figure 3(a) shows the time-averaged power absorption for each floater. As expected, the diagonal optimization (DO) method is more efficient than applying the optimal parameters of a single buoy to the array (OPSB). The power absorption is distributed very unequally between the buoys: the front buoys (in particular Nos 3 and 8) absorb about 2.7 times more energy than buoy No 7 in the back. Rather large buoy motions are observed in Figure 3(b), showing the significant amplitudes of the position of the buoys. Figures 3(c) and 3(d) present the external damping coefficients and supplementary mass coefficients, respectively.

If diagonal optimization is applied, the total power absorption is ca 400 kW. This corresponds to an increase with almost 50 kW compared to OPSB, as can be observed in Table 2. Although the power absorption of the array is large, the gain factor $\tilde{q}$ is rather small (46 %), since the absorbed power of an isolated buoy is quite large. It must be stressed, however, that this unconstrained case leads to considerable control forces (up to a value of $F_{tot,A,sign}$ of 400 kN) and floater motions, violating the assumptions behind linear theory. Consequently, these power absorption figures will most likely not be achieved in practical cases. Furthermore, the power absorption figures do not take into account losses due to mechanical friction,

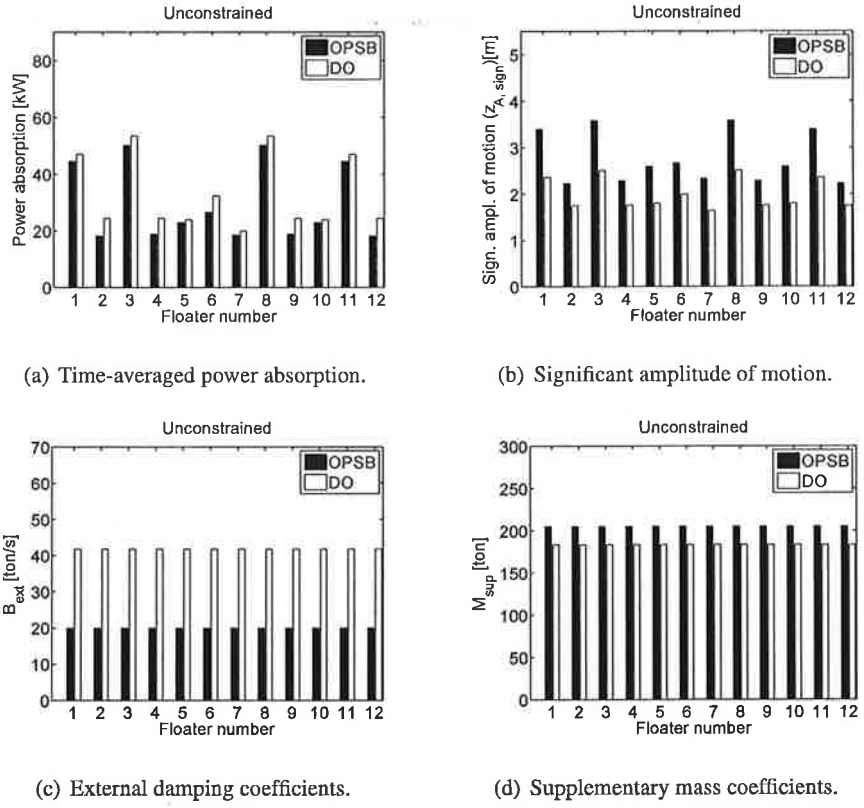

(a) Time-averaged power absorption.

(b) Significant amplitude of motion.

(c) External damping coefficients.

(d) Supplementary mass coefficients.

Figure 3: Simulation results in unconstrained conditions, with optimal control parameters for a single body and diagonal optimization, sea state: $H_s = 2.25$ m, $T_p = 7.22$ s.

viscous losses, turbine and generator losses or any other losses in the conversion system and hence, they do not correspond to the produced electrical power.

In unconstrained conditions, an individual tuning (IO) did not lead to any realistic solutions. Some buoys may be totally tuned towards resonance, oscillating with very large amplitudes, while other buoys are kept still. This is of course not a desired situation at all. Moreover, in unconstrained conditions the optimization algorithm has a large chance to find a local maximum instead of the absolute maximum, sometimes even without finding a solution which is symmetric with respect to the x-axis. More realistic, constrained cases will be addressed in the next Section.

4.2 Constrained

4.2.1 Slamming and Stroke constraint

The power absorption and gain factor are determined for the three optimization strategies, taking into account the slamming and stroke restrictions, as explained in Section 2.2. Table 2 shows that diagonal

optimization performs slightly better than the optimal parameters of a single body: the total power absorption is 381 kW with OPBS and 389 kW with DO. A significant benefit can be made by individually optimizing the control parameters of the floaters. The power absorption becomes 443 kW with IO, which is an increase of about 14 % compared to DO or an increase of 54 kW. This figure corresponds with the amount of power absorbed by an isolated buoy, and illustrates the large profit than can be made by individually tuning the buoys in case they are closely spaced. For the configurations evaluated in [17], the benefit of IO compared to DO was found to be less than one percent. This is most probably due to the fact that the floaters are wider spread from each other in [17]. The interdistance (centre-centre spacing) between two successive rows, for which the two methods were evaluated, varied between 3 and 4 times the diameter D, whereas in the present configuration the interdistance is about 1.3 D. The larger the interdistance, the more the behaviour of the buoy resembles that of an isolated buoy and the less difference will be found between the optimization techniques. Also the number of floaters is much smaller in [17]: five floaters are considered compared to twelve floaters in the present configuration. Particularly, the buoys in the back benefit considerably from an individual tuning, as is shown in Figure 4(a), presenting the power absorption for each buoy. Figure 4(b) shows the significant amplitude of the buoy motions. The external damping and tuning parameters are shown in Figures 4(c) and 4(d), respectively.

With IO, the power absorption is much better distributed among the floaters. A maximum factor of 2.6 is found between the individual power absorption of the front buoys and the rear buoys if DO is used, whereas only a factor of 1.9 is observed when IO is utilized. With individual optimization the buoys in the front absorb less power than with OPSB or DO, however, the buoys in the back become more efficient. This is realized by detuning the front buoys (small value of m_{sup} in Figure 4(d)), whereas the rear buoys, on the other hand, are tuned very well to increase their velocity amplitude and power absorption. Consequently, the power that is not absorbed anymore by the front buoys can be absorbed by the buoys in the rows behind them. This makes the influence of restrictions less drastic for an array than for a single buoy. These conclusions will be even more pronounced when the constraints are more stringent, as they will be in the next Sections.

All the buoys reach the maximum stroke value when IO is used, so the stroke restriction is dominant (Figure 4(b)). The slamming constraint is generally not critical in the presented examples for the given buoy dimensions and sea state.

4.2.2 Slamming, stroke and force constraint

In this Section the slamming and stroke restrictions are included together with the force constraint of 200 kN on the significant amplitude of the total control force. Figures 5(a)-5(d) give the power absorption, significant amplitude of the motion and the control parameters of each buoy. The significant amplitude of

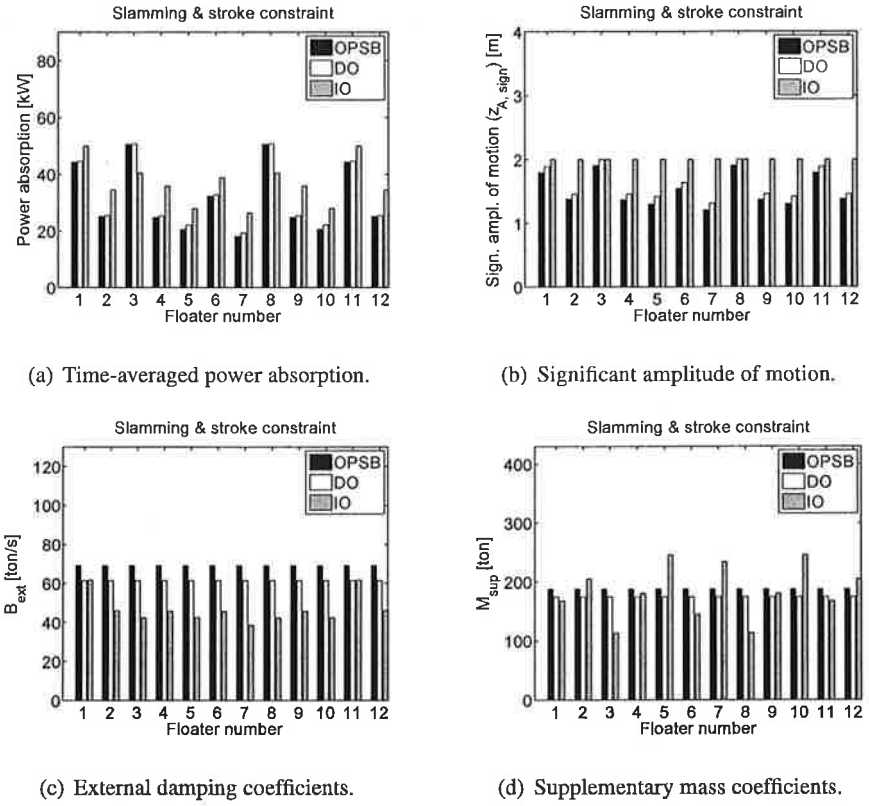

(a) Time-averaged power absorption.

(b) Significant amplitude of motion.

(c) External damping coefficients.

(d) Supplementary mass coefficients.

Figure 4: Simulation results in constrained conditions (slamming and stroke restriction), with optimal control parameters for a single body, diagonal and individual optimization, sea state: H_s = 2.25 m, T_p = 7.22 s.

the damping force, tuning force and total force are presented in Figures 5(e)-5(g) for the three optimization methods. The force constraint is clearly the most critical constraint. The buoy motions are considerably smaller than the stroke limit. The force limit on the other hand, is reached by the front buoys with the OPSB and DO methods and by all the buoys with IO. The front buoys even exceed the limit of 200 kN in case of OPSB. If certain control parameters meet the constraints for an isolated buoy, they do not necessarily satisfy the same restrictions applied to an array. This explains why more power is absorbed with OPSB (336 kW) than with the DO method (332 kW) in this case (see Table 2), although the DO method was found to be more efficient. Again, a large benefit can be made with the IO technique: the power absorption becomes 379 kW, corresponding with an increase of 46 kW compared to DO, which is even more than the power absorbed by an isolated buoy under the same constraints. Due to the extra force constraint, the power distribution among the floaters has been improved compared to the previous case; the buoys in the front absorb only about 50 % more than those in the back with IO, whereas with DO they absorb about double as

much than the rear buoys.

The gain factors $\tilde{q}$ have risen to 0.69 (DO) and 0.79 (IO) for this restriction case, although the total power absorption of the array has decreased due to the extra force constraint. This rise of $\tilde{q}$ can be attributed to the considerable power drop by an isolated buoy under these restrictions. An isolated buoy loses about 25 % of the power absorption, whereas the array loses only 12 to 14 %, compared to the slamming and stroke restriction case. Since the array suffers a bit less from the constraints than the isolated buoy, it has an increased relative performance, although the absolute performance is decreased.

4.2.3 Angle of wave incidence and effects of mistuning

So far, irregular waves propagating along the x-axis have been considered. It might be of interest to investigate the array behaviour for a different angle of wave incidence β_i, e.g. $\beta_i = 45°$. In that case, the configuration in Figure 1(b) can be considered as an aligned grid. The power absorption values and gain factors are presented in Table 2 for unconstrained motion as well as for the combination of slamming, stroke and force restrictions. It appears that the array performs slightly better when the incident waves propagate in the direction of the diagonal of the array (aligned grid), compared to normal incidence (staggered grid), however, the difference is not significant. The performance of an array is strongly dependent on the wave frequency and therefore the power absorption is calculated for the other sea states at Westhinder (as defined in Table 1). Figure 6 shows the gain factor $\tilde{q}$ versus the sea state for DO and IO and for two different angles of wave incidence ($\beta_i = 0°$ and, $\beta_i = 45°$), obtained with the slamming, stroke and force constraints. A steep rise in $\tilde{q}$-factor can be noticed from sea state 4 onwards. This might give the impression that the gain factor rises for longer waves. However, the increase is most probably caused by the constraints, which become important for the more energetic wave classes. Since a single body is relatively more affected by the constraints, the gain factor rises for more energetic waves.

In Figure 6 the difference between an angle of incidence of 0° and 45° is very minor for all sea states and no final conclusion can be made about the best angle of incidence. The difference in optimization strategy, on the other hand is very clear: for all sea states and both angles of incidence, individual optimization outperforms diagonal optimization.

In practice, there will be uncertainties on the characteristics of the sea state and the real sea state might not perfectly correspond to the values used in the numerical calculations. For instance the real spectrum might differ from the JONSWAP spectrum that has been employed, the current angle of wave incidence might not be known exactly, etc. Hence, it is important to have an idea of the sensitivity of the optimization techniques to mistuning effects. An example is given in Table 3 for unconstrained motion and one case of constrained conditions. Simulation results are presented for an angle of incidence of 45°, but the optimal control parameters (CP) are taken from the simulations with normal wave incidence. It is expected that

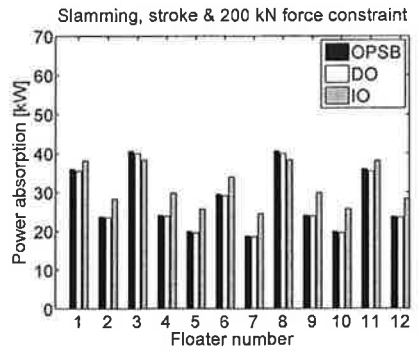

(a) Time-averaged power absorption.

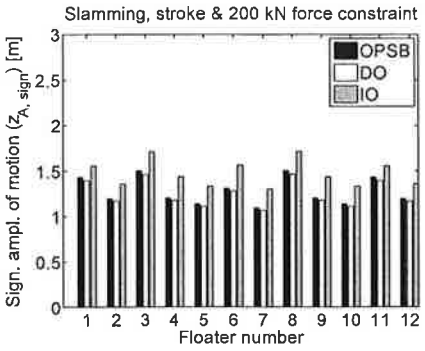

(b) Significant amplitude of motion.

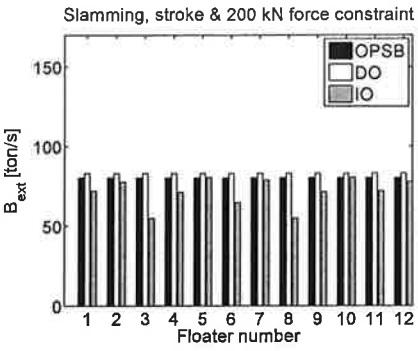

(c) External damping coefficients.

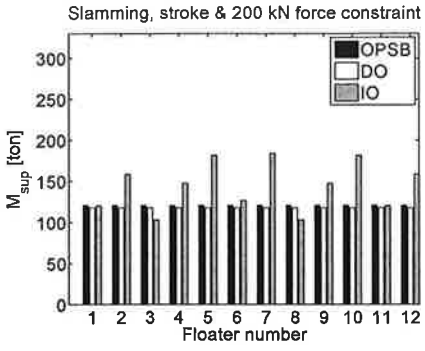

(d) Supplementary mass coefficients.

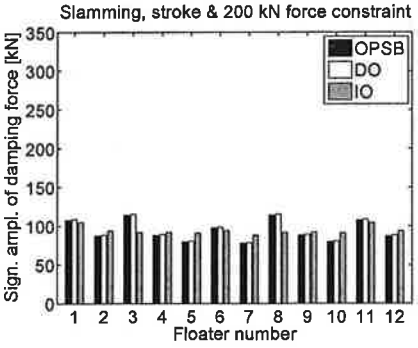

(e) Significant amplitude of damping force.

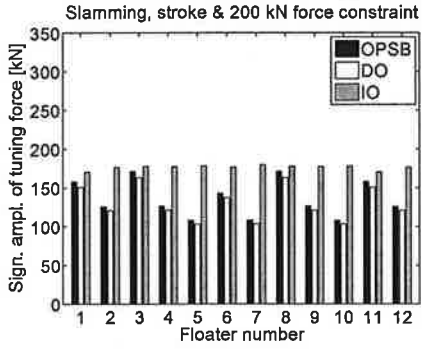

(f) Significant amplitude of tuning force.

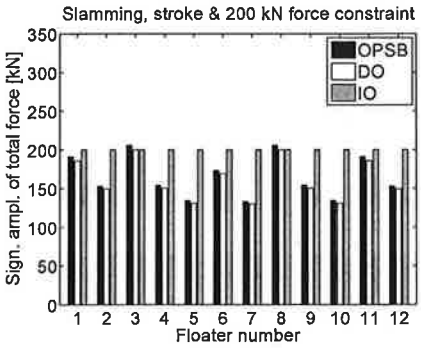

(g) Significant amplitude of total control force.

Figure 5: Simulation results in constrained conditions (slamming and stroke restriction, and force restriction: $F^{(j)}_{tot,A,sign} \leq 200$ kN), with optimal control parameters for a single body, diagonal and individual optimization, sea state: $H_s = 2.25$ m, $T_p = 7.22$ s.

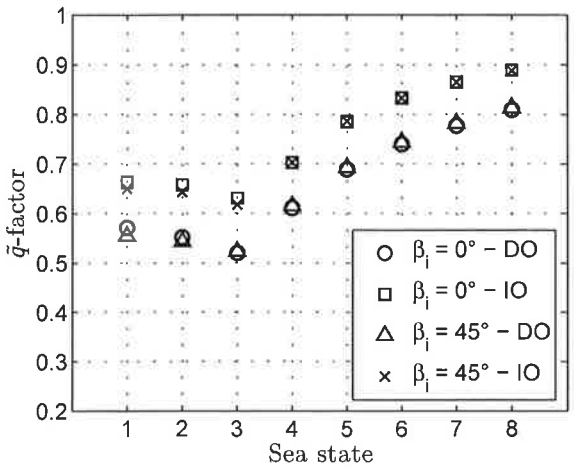

Figure 6: $\tilde{q}$-factors for diagonal and individual optimization as a function of the nine sea states on the Belgian Continental Shelf, configuration: 12 buoys, constraints: slamming, stroke and force restriction.

for the individually optimized parameters, the effect of mistuning will be more pronounced than for the diagonally optimized parameters. This appears to be correct, however, the effect of mistuning is extremely small. For DO the difference in power absorption is less than 0.50 % compared to the results with the correct control parameters for $\beta_i = 45°$. For IO this difference is 1.76 % for the studied case. Obviously, the larger the mistuning, the larger will be the impact on the power absorption, in particular for IO.

It needs to be mentioned that with the mistuned parameters, the force constraint is still fulfilled for DO, but not anymore for IO. The problem is caused by buoy No 12, exceeding the force limit by 20 %. The buoy is tuned as a rear buoy ($\beta_i = 0°$), getting a high value of the supplementary mass, and becomes rather a front buoy when $\beta_i = 45°$, where it is subjected to higher incident waves. The combination of an increased supplementary mass and large buoy motion parameters leads to larger control forces. When these control forces cannot be delivered, the power absorption figures will be less than expected and hence, the aforementioned losses due to mistuning effects will be larger. More serious problems might be expected when slamming or stroke restrictions are violated. In that case, not only the performance of the system will diminish, but also the lifetime of the device might be affected, due to heavily slamming of the floater on the water surface or e.g. on the fenders attached to the structure enclosing the point absorber.

Table 2: Absorbed power and gain factor $\tilde{q}$ for unconstrained and constrained cases, 12 buoys configuration.

Sea state:	Single body (SB)	Multiple bodies (MB)					
$H_s = 2.25$ m, $T_p = 7.22$ s		OPSB		DO		IO	
Constraints	NP_{abs} [kW]	P_{abs} [kW]	$\tilde{q}$ [-]	P_{abs} [kW]	$\tilde{q}$ [-]	P_{abs} [kW]	$\tilde{q}$ [-]
$\beta_i = 0°$							
Unconstrained	872	354	0.41	399	0.46	-	-
Slam, stroke 2.00 m	645	381	0.59	389	0.60	443	0.69
Slam, stroke 2.00 m, force 200 kN	482	336	0.70	332	0.69	379	0.79
$\beta_i = 45°$							
Unconstrained	872	360	0.41	403	0.46	-	-
Slam, stroke 2.00 m, force 200 kN	482	337	0.70	334	0.69	379	0.79

Table 3: Effects of mistuning - power absorption for the 12 buoy configuration, with $\beta_i = 45°$, while the control parameters (CP) are those obtained for $\beta_i = 0°$.

Sea state:						
$H_s = 2.25$ m, $T_p = 7.22$ s	DO			IO		
Constraints	P_{abs} [kW]	$\tilde{q}$ [-]	Power loss [%]	P_{abs} [kW]	$\tilde{q}$ [-]	Power loss [%]
$\beta_i = 45°$, CP from $\beta_i = 0°$						
Unconstrained	403	0.46	0.01	-	-	
Slam, stroke 2.00 m, force 200 kN	333	0.69	0.45	372	0.77	1.76

4.2.4 Application to the Belgian Continental Shelf

Figure 7 gives the power absorption versus the sea states at Westhinder for the configuration with 12 and 21 floaters for individual optimization of the control parameters, considering the slamming, stroke and force constraints. The results are based on unidirectional, irregular head-on waves ($\beta_i = 0°$). It is observed from the graph that the power absorption rises swiftly as the sea states become more energetic. When combining the power absorption numbers of Figure 7 with the occurrence frequencies of the sea states at Westhinder (mentioned in Table 1), the absorbed energy over a certain period of time can be determined. The results are shown in Table 4 for the layouts with 12 and 21 bodies both with diagonal and individual optimization of the control parameters. The energy absorption values are presented relative to the energy absorbed by the 12 buoy configuration with DO. Note again the benefit of applying individual optimization of the control parameters. The energy absorption is increased with approximately 16 % and 18 % for the layout with 12 buoys and 21 buoys, respectively.

Table 4: Absorbed energy at Westhinder for the configurations with 12 and 21 buoys, both with DO and IO. The data has been normalized by the energy absorption from the 12 buoy layout with DO. Constraints: slamming, stroke and force constraint.

	12 buoys		21 buoys	
	DO	IO	DO	IO
Energy absorption [-]	1.00	1.16	1.23	1.45
Truncated energy absorption [-]	0.94	1.10	1.16	1.37

Figure 8 shows the contribution of each sea state to the power absorption for the two considered configurations with individual optimization. The share in the average power absorption of the larger sea states is huge compared to the smaller sea states. Note that the smallest sea state, which has an occurrence frequency of more than 20 %, has almost no contribution to the power absorption. It might be of interest to truncate the power absorption at a certain sea state, since the power levels corresponding to the most energetic sea states might be very large, resulting in a costly design of the power take-off system. An example is presented in which the power absorption values of sea state 5 are considered as the upper limit, or alternatively, the average power absorption of sea states 6 to 8 equals that of sea state 5. Note that the average power absorption values are truncated and that the instantaneous, rated power values are still larger. The energy absorption values for the truncated case are also presented in Table 4. The effect of the truncation is rather small.

Based on these preliminary calculations, the benefit of exploiting a device with 21 floaters (of diameter 4 m) versus 12 floaters (of diameter 5 m) appears to be rather limited. The average power absorption is increased with only 23 to 25 % if 21 floaters with a 4 m diameter are installed compared to the 12 floaters with a larger diameter. A device with 12 floaters is less complex and is therefore expected to be less expensive. Hence, it is important to combine results of the hydrodynamic performance with cost estimates before a final conclusion can be made on the entire performance of different arrays.

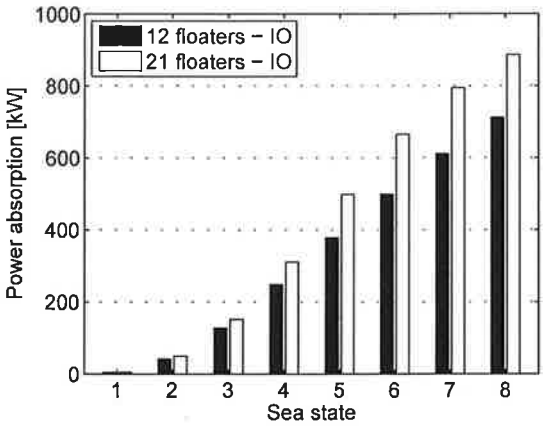

Figure 7: Power absorption per sea state for the configuration with 12 and 21 buoys. Constraints: slamming, stroke and force constraint.

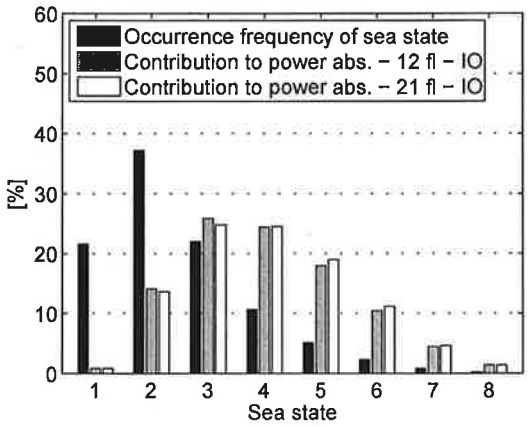

Figure 8: Occurrence frequency of sea states and the percentual contribution of each sea state to the power absorption for both array configurations. Constraints: slamming, stroke and force constraint.

5 Conclusion

The behaviour of closely spaced point absorbers in unconstrained and constrained conditions has been analysed in unidirectional irregular waves. Two array layouts are considered: 12 buoys with a diameter of 5 m in a staggered grid and 21 buoys with a diameter of 4 m in an aligned grid. The buoys are assumed to be equipped with a linear power take-off, consisting of a linear damping and a linear tuning force. In unconstrained conditions the absorbed power is found to be very unequally distributed among the floaters. For the considered sea state and the 12 buoys configuration, the front buoys absorbed 2.7 times more power than the rear buoys in unconstrained conditions. For the most stringent constraints the difference was reduced to a factor of 1.5 to 2. The total power absorption of the array is negatively affected by the implementation of constraints. However, it is observed that the relative power loss of the array is less than for a single body, since mainly the front buoys are affected by the constraints and to a lesser extent the rear buoys. The power absorption of the arrays has been determined in three different ways. Firstly, the optimal parameters of a single body are applied to the array. This turns out not to be an efficient way. Moreover, the constraints were not always fulfilled for all the bodies in the array, although they were satisfied for the single body case. Secondly, diagonal optimization has been applied. With this method all buoys have the same control parameters, but they are optimized for the array. In the third method, the buoys get individually optimized control parameters. This strategy clearly outperforms the two other methods. At Westhinder on the Belgian Continental Shelf, the energy absorption is increased by 16 % and 18 %, respectively, for the configurations with 12 and 21 buoys, by individually optimizing the control parameters, compared to diagonally optimizing them. It is found that the average energy absorption at Westhinder for the 21 buoys with diameter 4 m is only one quarter larger than for the 12 buoys with diameter 5 m. As it is expected that the latter configuration will be less expensive than the layout with 21 buoys, it would be useful for future work to take into account a cost estimate in order to evaluate the different configurations. Furthermore, it would be relevant to compare the performance of the different control strategies applied in short-crested waves with the presented findings based on long-crested waves.

References

[1] Bjerrum A., The Wave Star Energy concept. In: 2nd International Conference on Ocean Energy, 2008.

[2] http://www.manchesterbobber.com/.

[3] Taghipour R., Arswendy A., Devergez M., Moan T., Efficient frequency-domain analysis of dynamic response for the multi-body wave energy converter in multi-directional waves. In: The 18th International Offshore and Polar Engineering Conference, 2008.

[4] Budal K., Theory for absorption of wave power by a system of interacting bodies. Journal of Ship Research 1977;21:248–253.

[5] Evans D., Some analytic results for two- and three-dimensional wave-energy absorbers. B. Count: Academic Press, 1980.

[6] Falnes J., Radiation impedance matrix and optimum power absorption for interacting oscillators in surface waves. Applied Ocean Research 1980;2:75–80.

[7] Mavrakos S., Kalofonos A., Power absorption by arrays of interacting vertical axisymmetric wave-energy devices. Journal of Offshore Mechanics and Arctic Engineering - Transactions of the ASME 1997;119:244–251.

[8] Simon J., Multiple scattering in arrays of axisymmetric wave-energy devices. Part 1. A matrix method using a plane-wave approximation. Journal of Fluid Mechanics 1982;120:1–25.

[9] McIver P., Evans D., Approximation of wave forces on cylinder arrays. Applied Ocean Research 1984; 6:101–107.

[10] McIver P., Wave forces on arrays of bodies. Journal of Engineering and Mathematics 1984;18:273–285.

[11] Kagemoto H., Yue D., Interactions among multiple three-dimensional bodies in water waves: an exact algebraic method. Journal of Fluid Mechanics 1986;166:189–209.

[12] McIver P., Some hydrodynamic aspects of arrays of wave-energy devices. Applied Ocean Research 1994;16:61–69.

[13] McIver P., Mavrakos S.A., Singh G., Wave-power absorption by arrays of devices. In: 2nd European Wave Power Conference, Portugal, 1995, pp. 126–133.

[14] Thomas S., Weller S., Stallard T., Comparison of numerical and experimental results for the response of heaving floats within an array. In: 2nd International Conference on Ocean Energy, France, 2008.

[15] Mavrakos S.A., Hydrodynamic coefficients for groups of interacting vertical axisymmetric bodies. Ocean Engineering 1991;18:485–515.

[16] Mavrakos S.A., McIver P., Comparison of methods for computing hydrodynamic characteristics of arrays of wave power devices. Applied Ocean Research 1997;19:283–291.

[17] Ricci P., Saulnier J.B., Falcao A., Point-absorber arrays: a configuration study off the Portuguese west-coast. In: 7th European Wave and Tidal Energy Conference, Portugal, 2007.

[18] WAMIT user manual: http://www.wamit.com/manual.htm.

[19] Cruz J., Sykes R., Siddorn P., Eatock Taylor R., Wave farm design: Preliminary studies on the influences of wave climate, array layout and farm control. In: 8th European Wave and Tidal Energy Conference, Sweden, 2009, pp. 736–745.

[20] Babarit A., Borgarino B., Ferrant P., Clément A., Assessment of the influence of the distance between two wave energy converters on the energy production. In: 8th European Wave and Tidal Energy Conference, Sweden, 2009, pp. 528–537.

[21] De Backer G., Vantorre M., Banasiak R., De Rouck J., Beels C., Verhaeghe H., Performance of a point absorber heaving with respect to a floating platform. In: 7th European Wave and Tidal Energy Conference, Portugal, 2007.

[22] De Backer G., Vantorre M., Beels C., De Rouck J., Frigaard P., Performance of closely spaced point absorbers with constrained floater motion. In: 8th European Wave and Tidal Energy Conference, Sweden, 2009, pp. 806–817.

[23] Budal K., Falnes J., Interacting point absorbers with controlled motion, in Power from Sea Waves. B. Count: Academic Press, 1980.

[24] Vantorre M., Banasiak R., Verhoeven R., Modelling of hydraulic performance and wave energy extraction by a point absorber in heave. Applied Ocean Research 2004;26:61–72.

[25] Peseux B., Gornet L., Donguy B., Hydrodynamic impact: Numerical and experimental investigations. Journal of Fluids and Structures 2005;21(3):277–303.

[26] Goda Y., Random seas and design of maritime structures. World Scientific Publishing Co, 2008.